AFRL-RZ-WP-TP-2010-2217

INTEGRATED NONLINEAR DYNAMIC MODELING AND FIELD ORIENTED CONTROL OF PERMANENT MAGNET (PM) MOTOR FOR HIGH PERFORMANCE EMA (PREPRINT)

David Woodburn, Thomas Wu, Shaohua Lin, Jared Bindl, Yang Hu, Wendell Brokaw, Louis Chow, Lei Zhou, and Yeong-Ren Lin

University of Central Florida

Quinn Leland, Ben Tran, Brett Jordan, Earl Gregory, and Steve Iden

Mechanical Energy Conversion Branch
Energy/Power/Thermal Division

Nicholas Rolinski

University of Dayton Research Institute

NOVEMBER 2010

AIR FORCE RESEARCH LABORATORY
PROPULSION DIRECTORATE
WRIGHT-PATTERSON AIR FORCE BASE, OH 45433-7251
AIR FORCE MATERIEL COMMAND
UNITED STATES AIR FORCE

REPORT DOCUMENTATION PAGE

Form Approved
OMB No. 0704-0188

1. REPORT DATE *(DD-MM-YYYY)*	2. REPORT TYPE	3. DATES COVERED *(From - To)*
November 2010	Conference Paper Preprint	21 Feb 2009 – 02 Nov 2010

4. TITLE AND SUBTITLE
INTEGRATED NONLINEAR DYNAMIC MODELING AND FIELD ORIENTED CONTROL OF PERMANENT MAGNET (PM) MOTOR FOR HIGH PERFORMANCE EMA (PREPRINT)

5a. CONTRACT NUMBER
In-House

5b. GRANT NUMBER

5c. PROGRAM ELEMENT NUMBER
62203F

6. AUTHOR(S)
David Woodburn, Thomas Wu, Shaohua Lin, Jared Bindl, Yang Hu, Wendell Brokaw, Louis Chow, Lei Zhou, and Yeong-Ren Lin (University of Central Florida)

Quinn Leland, Ben Tran, Brett Jordan, Earl Gregory, and Steve Iden (AFRL/RZPG)
Nicholas Rolinski (University of Dayton Research Institute)

5d. PROJECT NUMBER
3145

5e. TASK NUMBER
13

5f. WORK UNIT NUMBER
31451313

7. PERFORMING ORGANIZATION NAME(S) AND ADDRESS(ES)

University of Central Florida
4000 Central Florida Boulevard
Orlando, FL 32816

University of Dayton Research Institute
300 College Park
Dayton, OH 45469

Mechanical Energy Conversion Branch (AFRL/RZPG)
Energy/Power/Thermal Division
Air Force Research Laboratory, Propulsion Directorate
Wright-Patterson Air Force Base, OH 45433-7251
Air Force Materiel Command, United States Air Force

8. PERFORMING ORGANIZATION REPORT

9. SPONSORING / MONITORING AGENCY NAME(S) AND ADDRESS(ES)

Air Force Research Laboratory
Propulsion Directorate
Wright-Patterson Air Force Base, OH 45433-7251
Air Force Materiel Command
United States Air Force

10. SPONSOR/MONITOR'S ACRONYM(S)
AFRL/RZPG

11. SPONSOR/MONITOR'S REPORT NUMBER(S)
AFRL-RZ-WP-TP-2010-2217

12. DISTRIBUTION / AVAILABILITY STATEMENT
Approved for public release; distribution unlimited.

13. SUPPLEMENTARY NOTES
Conference paper presented at the Power Systems Conference, November 2010, in Fort Worth, TX. This paper contains color. PA Case Number: 88ABW-2010-3024; Clearance Date: 03 Jun 2010.

14. ABSTRACT
This paper describes the integrated modeling of a permanent magnet (PM) motor used in an electromechanical actuator (EMA). A nonlinear, lumped-element motor electric model is detailed. The parameters, including nonlinear inductance, rotor flux linkage, and thermal resistances, and capacitances, are tuned using FEM models of a real, commercial motor. The field-oriented control (FOC) scheme and the lumped-element thermal model are also described.

15. SUBJECT TERMS:
integrated, nonlinear, dynamic, field oriented control, permanent magnet, EMA, electromechanical actuator, lumpedelement model, inductance, flux linkage, all-electric aircraft, coenergy, eddy current, three phase, convergence, directquadrature reference frame, windage, hysteresis, classical eddy, excess eddy, line simplification, heat generation, adaptive, feedback linearization, PI

16. SECURITY CLASSIFICATION OF:			17. LIMITATION OF ABSTRACT	18. NUMBER OF PAGES	19a. NAME OF RESPONSIBLE PERSON
a. REPORT	b. ABSTRACT	c. THIS PAGE			Quinn Leland
Unclassified	Unclassified	Unclassified	SAR	22	19b. TELEPHONE NUMBER *(include area code)* 937-255-3060

10PSC-0110

Integrated Nonlinear Dynamic Modeling and Field Oriented Control of Permanent Magnet (PM) Motor for High Performance EMA

David Woodburn, Thomas Wu, Shaohua Lin, Jared Bindl, Yang Hu, Wendell Brokaw
School of Electrical Engineering and Computer Science, University of Central Florida

Louis Chow, Lei Zhou, Yeong-Ren Lin
Department of Mechanical, Materials, and Aerospace Engineering, University of Central Florida

Quinn Leland, Ben Tran, Brett Jordan, Earl Gregory, Steve Iden
Air Force Research Laboratory, Wright-Patterson AFB

Nicholas Rolinski
Department of Mechanical Engineering, University of Dayton

ABSTRACT

This paper describes the integrated modeling of a permanent magnet (PM) motor used in an electromechanical actuator (EMA). A nonlinear, lumped-element motor electric model is detailed. The parameters, including nonlinear inductance, rotor flux linkage, and thermal resistances, and capacitances, are tuned using FEM models of a real, commercial motor. The field-oriented control (FOC) scheme and the lumped-element thermal model are also described.

INTRODUCTION

The development of all-electric aircraft is a high priority in the avionics community. Current aircraft use a combination of hydraulic, pneumatic, and electric systems for flight control. However, the expectation for future airplanes is a single, electric system using electromechanical actuators (EMAs). Such a system would reduce the cost to build, operate, and maintain aircraft. It would also make aircraft lighter, more reliable, safer, and more easily reconfigurable, reducing the turnaround for new technology [1].

One of the greatest hurdles to replacing all hydraulic actuators with EMAs is the removal of heat generated within them, a consequence of the absence of cooling hydraulic fluid. Accurately quantifying the heat generated is complicated by the highly transient and localized nature of the power demands of an EMA's motor, an especially significant issue in aircraft. Thus, accurate modeling must be dynamic.

The parameters that characterize a motor, such as resistance and inductance, are actually nonlinear functions. In steady-state analysis, these nonlinearities can simply be averaged out, and often the parameters are considered to be constant [2]. But during transient analysis these nonlinearities can become critical [3]. Consequently, time-averaged, linear models [4] are inadequate for thermal analysis and management designs. So, proper treatment of the problem requires dynamic, nonlinear analysis.

The motor parameters can be determined by careful experimentation [3-4], but this is a time intensive process and can be expensive especially when considering multiple potential designs for a motor. Jens Otto suggested using a reduced order coenergy model [5], which yielded results comparable to FEM results. Likewise, Roshen considered more involved empirical formulas which accounted for excess eddy current losses [6].

Through FEM modeling, the nonlinear parameters, such as self and mutual inductances of the three phase windings, can be determined [7-8]. Though dynamic FEM can be very accurate [5], such detailed simulation is very slow. Fortunately, FEM is only necessary to quantify the parameters; it is not necessary for simulating the motor over lengthy mission profiles. Instead, a nonlinear, lumped element model (NL-LEM) can use the parameters from the FEM model and then dynamically simulate the motor just as accurately as the FEM model but at a much lower computational cost. Our paper addresses the nonlinear dynamic modeling of a permanent magnet motor and describes both the control and thermal performance of the motor in following highly transient input mission profiles.

MODEL

Two inputs are given: a time-history profile (a sequence of data points versus time) of desired positions (stroke reference profile) and another time-history profile of load forces (force profile). Both of these profiles can be translated to the perspective of the motor through the conversion factor of the drive train ratio so that we get a rotor angle profile and a load torque profile. Then, for each time step, the appropriate applied voltages to make the motor follow the stroke profile in the presence of the load torque profile are calculated by the control algorithm. These voltages are then applied to the motor, at which point the simulation enters a convergence loop to determine what the correct currents and motor-generated torques would be in the presence of such applied voltages. With the motor-generated torque determined, the new rotor position can be calculated for that time step. Thus, the motion of the motor is simulated. Now, for each time step, once the currents are calculated, the power loss in the windings can also be found. These copper power losses then become the heat sources for the thermal algorithm, where temperatures for various points (nodes) in the motor are calculated. The outputs from the simulation are the actual stroke profile of the motor (as opposed to what was desired: the reference profile), the electrical power flowing in and out (regen) of the motor, and the temperature profiles for the various nodes.

SIMULATION EQUATIONS

The motor dynamics are modeled by four primary dynamical equations in direct-quadrature reference frame (dq0) [9]. The first two of these four are shown here:

$$u_d = R_s i_d + \frac{d\lambda_d}{dt} - \omega_{me}\lambda_q \qquad (1)$$

$$u_q = R_s i_q + \frac{d\lambda_q}{dt} + \omega_{me}\lambda_d, \qquad (2)$$

where u_d is input direct voltage, u_q is input quadrature voltage, i_d is direct current, i_q is quadrature current, λ_d is direct flux linkage, λ_q is quadrature flux linkage, R_s is phase resistance, ω_{me} is the mechanical frequency multiplied by the number of pole pairs $p/2$, and p is the number of poles. The two variables λ_d and λ_q can be expressed by

$$\lambda_d = L_d(i_q, i_d)i_d + \lambda_{PM} \quad (3)$$

$$\lambda_q = L_q(i_q, i_d)i_q, \qquad (4)$$

where λ_{PM} is the flux linkage from the permanent magnet, which is a constant. Therefore, the time-derivatives of these two flux linkages would be the following:

$$\frac{d\lambda_d}{dt} = L_d(i_q, i_d)\frac{di_d}{dt} + \frac{dL_d(i_q, i_d)}{di_q}\frac{di_q}{dt}i_d + \frac{dL_d(i_q, i_d)}{di_d}\frac{di_d}{dt}i_d \qquad (5)$$

$$\frac{d\lambda_q}{dt} = L_q(i_q, i_d)\frac{di_q}{dt} + \frac{dL_q(i_q, i_d)}{di_q}\frac{di_q}{dt}i_q + \frac{dL_q(i_q, i_d)}{di_d}\frac{di_d}{dt}i_q, \qquad (6)$$

For PM motors in EMA applications, we can design the controller to keep the direct current close to zero. Also, the change in L_d and L_q will change only slightly with current, for our particular motor. Therefore, in equations (5) and (6), the second and third terms can be dropped, leaving us with

$$\frac{d\lambda_d}{dt} \approx L_d(i_q, i_d)\frac{di_d}{dt} \qquad (7)$$

$$\frac{d\lambda_q}{dt} \approx L_q(i_q, i_d)\frac{di_q}{dt}, \quad (8)$$

With these changes, equations (1) and (2) can be modified to the form of (9) and (10), which along with equations (11) and (12) are our four primary dynamical equations.

$$\frac{di_d}{dt} = \frac{1}{L_d}\left(u_d - R_s i_d + \omega_{me} L_q i_q\right) \qquad (9)$$

$$\frac{di_q}{dt} = \frac{1}{L_q}\left(u_q - R_s i_q - \omega_{me} L_d i_d - \omega_{me}\lambda_{PM}\right) \qquad (10)$$

$$\frac{d\omega_{me}}{dt} = \frac{1}{I}\left[\frac{p}{2}\left(\tau_M - \tau_L\right) - c\omega_{me}\right] \qquad (11)$$

$$\frac{d\theta_{me}}{dt} = \omega_{me}, \quad (12)$$

where τ_L is the load torque, θ_{me} is the mechanical angle multiplied by the number of pole pairs $p/2$, I is the rotor's moment of inertia, c is the rotor's coefficient of friction from windage and bearings, and τ_M is the motor torque generated by the magnetic fields and is given by

$$\tau_M = i_q\left\{\frac{3}{4}p\cdot\left[\lambda_{PM} + i_d\cdot\left(L_d - L_q\right)\right]\right\}. \quad (13)$$

The motor losses are related to the motor parameters, such as R_s, c, L_d, and L_q. Since losses have an effect on motor behavior, when possible they should be modeled through the motor parameters, not calculated in post-processing, as is often done [6]. The copper loss can be calculated as

$$P_{cu} = \left(i_a{}^2 + i_b{}^2 + i_c{}^2\right)R_s, \qquad (14)$$

or equivalently

$$P_{cu} = \frac{3}{2}\left(i_d{}^2 + i_q{}^2\right)R_s, \quad (15)$$

for balanced 3-phases. The electrical phase resistance is itself a function of temperature. The relationship between R_s and R_{s0}, the phase resistance at room temperature, is as follows:

$$R_s = R_{s0}\frac{\rho}{\rho_0}, \quad (16)$$

where ρ_0 is the resistivity of copper at room temperature and ρ is the resistivity of copper at any temperature, *T*, given as

$$\rho\ [\mathrm{n\Omega\cdot m}] = 15.4[1 + 0.00451(T - 273[\mathrm{K}])]. \quad (17)$$

In either case, note that the resistance is the parameter directly associated with the power loss in the windings (the copper loss). Likewise, windage and bearing losses are directly associated with the coefficient of friction, c. All iron losses (hysteresis, classical eddy, and excess eddy losses) could be associated with nonlinear, hysteretic inductances, L_d and L_q.

Much of the motor modeling research done in the past [2] and [10] and even recent work [11] uses constant parameter values in simulations, although some did use nonlinear inductances [3] and [8], and [12]. Since the BH curve is nonlinear and H is a function of current, inductance is also a nonlinear function of current. For our model, we used FEM to obtain L_d and L_q as functions of i_q. At this point we are neglecting changes in i_d since our control algorithm already seeks to maintain a zero value for i_d. The inductance curves were calculated in ANSYS using the magnetization curve for the steel-1018 soft-magnetic material and the geometry of our motor. The analysis was done for zero direct current and for a wide range of quadrature currents (Fig. 1).

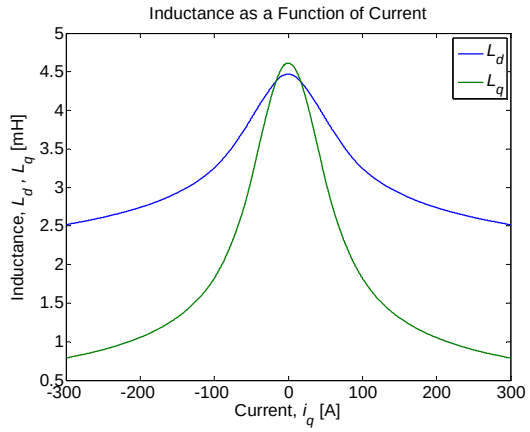

Fig. 1. Direct and quadrature inductances as functions of quadrature current

TIME STEPPING

The size of variable arrays of data points affects the speed of a simulation. Using prerecorded input profiles (time-history arrays of stroke and load torque), very small time stepping is necessary to accurately capture the transient behavior in the motor. A uniformly applied, very small time stepping would result in very large data arrays. To keep our array sizes small while maintaining small time stepping where needed, we used a line simplification algorithm to reduce the number of points where little transient activity would occur. This data compression technique allowed us to reduce the input profiles to less than 4% of their original data size.

That said, the electrical time constant is often much smaller than the smallest time step of the input profiles. Since the frequency of the electrical component of the simulation is directly related to the first derivative of the input angular position profile for the motor, we can dynamically scale the electrical time step non-uniformly [13]. Therefore, we had two loops, one macro loop that stepped through the elements of the input stroke profile and a nested micro loop with very small, but variable time steps for the electrical equations. The result of this apparent complication was a significant speed improvement.

FIELD ORIENTED CONTROL (FOC)

A thorough analysis of motor heat generation should include how the motor is driven. Our field oriented control is shown in Fig. 2, where the numbers in parenthesis refer to the equations shown further below. The control is an adaptive closed-loop control, which is a type of feedback linearization of the speed and position errors.

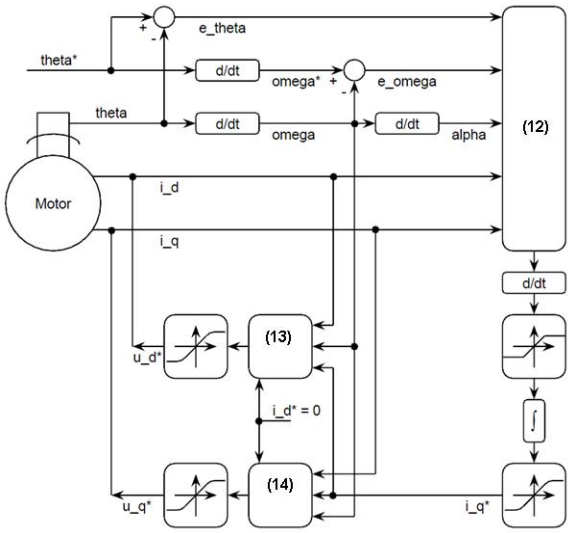

Fig. 2. Field oriented control (FOC) of PM motor

Our control equations are derived from the primary simulation equations (9) through (12). Starting with equation (11) and noting that in (13) i_q can be factored out, we get

$$i_q \frac{\tau_M}{i_q} = \tau_L + \frac{2}{p}\left(I\alpha_{me} + c\omega_{me}\right), \quad (18)$$

where, the angular acceleration multiplied by the number of pole pairs $p/2$, α_{me}, is defined as time derivative of ω_{me}. Equation (18) can be rearranged to be

$$i_q = \frac{\tau_L + \frac{2}{p}\left(I\alpha_{me} + c\omega_{me}\right)}{\frac{\tau_M}{i_q}}. \quad (19)$$

At this point we reinterpret α_{me} which is $d\omega_{me}/dt$ to be $e_{\omega_{me}}/\Delta t$, where Δt is a finite time step and $e_{\omega_{me}}$ is the error in ω_{me}, with a tuning coefficient, k_p, in front. This gives

$$i_q^* = \frac{\tau_L + \frac{2}{p}\left(Ik_p \frac{e_{\omega_{me}}}{\Delta t} + c\omega_{me}^* \right)}{\frac{\tau_M}{i_q}}, \qquad (20)$$

where i_q^* is the desired current for the next time step and ω_{me}^* is the desired next-step angular speed equal to $\omega_{me} + k_p e_{\omega_{me}}$. Using (11) to substitute for τ_L in (20), we arrive at (21):

$$i_q^* = \frac{\left(\tau_M - \frac{2}{p} I\alpha_{me} - \frac{2}{p} c\omega_{me} \right)}{\frac{\tau_M}{i_q}} + \frac{\frac{2}{p}\left(Ik_p \frac{e_{\omega_{me}}}{\Delta t} + c\omega_{me}^* \right)}{\frac{\tau_M}{i_q}}. \qquad (21)$$

Recalling that $\left(\omega_{me}^* - \omega_{me}\right)$ equals $k_p e_{\omega_{me}}$, (21) simplifies to

$$i_q^* = i_q + \frac{2}{p\frac{\tau_M}{i_q}}\left[I\left(k_p \frac{e_{\omega_{me}}}{\Delta t} - \alpha_{me} \right) + c\left(k_p e_{\omega_{me}}\right) \right], \qquad (22)$$

This equation will track the desired motor velocity well, but there will be some rotor angle drift over time. To counter this drift error, we added a theta error term, $k_i e_{\theta_{me}} / \Delta t$:

$$i_q^* = i_q + \left(k_i \frac{e_{\theta_{me}}}{\Delta t} \right) + \frac{2}{p\frac{\tau_M}{i_q}}\left[I\left(k_p \frac{e_{\omega_{me}}}{\Delta t} - \alpha_{me} \right) + c\left(k_p e_{\omega_{me}}\right) \right]. \qquad (23)$$

The k_p and k_i coefficients are the only PI (proportional integral) values that need to be tuned in the control algorithm. The coefficient k_p scales the controller's reaction to the error in ω_{me}, and k_i scales the controller's reaction to error in θ_{me}, the motor angle multiplied by the number of pole pairs. Together, these two coefficients help us set how quickly the controller will try to eliminate the particular error.

For maximum efficiency, it is generally desired that the direct current be zero since any flux generated in the direct axis would not contribute to torque. However, direct current does not necessarily directly translate to direct flux. Direct current can contribute to useful torque if the direct and quadrature inductances are not equal, as given in (13).

Most of the time, however, the desired direct current set point, i_d^*, should be zero. With the desired currents determined, the desired voltages can be found:

$$u_d^* = R_s i_d^* + L_d^* \frac{di_d^*}{dt} - \omega_{me}^* L_q^* i_q^* \quad (24)$$

$$u_q^* = R_s i_q^* + L_q^* \frac{di_q^*}{dt} + \omega_{me}^* L_d^* i_d^* + \omega_{me}^* \lambda_{PM}, \quad (25)$$

where L_d^* and L_q^* are based on the desired current values. It should be noted that while many of the variables are updated based upon the desired currents, τ_M was not updated for the control equations. This is a reasonable simplification since for a round rotor λ_{PM} is independent of θ_{me}, i_d should normally be zero, and the i_q factor is divided out:

$$\frac{\tau_M}{i_q} = \frac{3}{4} p \cdot \left[\lambda_{PM} + i_d \cdot \left(L_d - L_q\right)\right] \quad (26)$$

For the non-round rotor case, a direct interpolation method with a lookup table could be used to include the dependence on theta.

Even after the desired control values were calculated, the reality of limits (current and voltage) needed to be included. Instead of directly capping those values, we realized that the system converged more quickly and ran more smoothly if the functions used were all smooth [14]. For our case, we used a smooth, segmented curve of first and second-order polynomials to define the saturation of voltages.

TEMPERATURE CALCULATION

Using a lumped-element thermal model, the temperatures at 12 different locations (Refer to nodes 1, 3-10, and 12-14 in Fig. 3) in the motor were calculated. Similar work has been done before [15], though with only one node. The source of heat for the temperature calculations was the copper power loss in the windings. The temperature distribution of the motor was modeled using a lumped-element network (Fig. 3), which is limited to what is inside the motor assembly (indicated by the dashed line in Fig. 3). The heat transfer coefficient used, h, was 1.45 W/K m^2. The values of the thermal resistances and capacitances were tuned by comparing the results of the lumped-element model with those of an ANSYS FEM model of the motor.

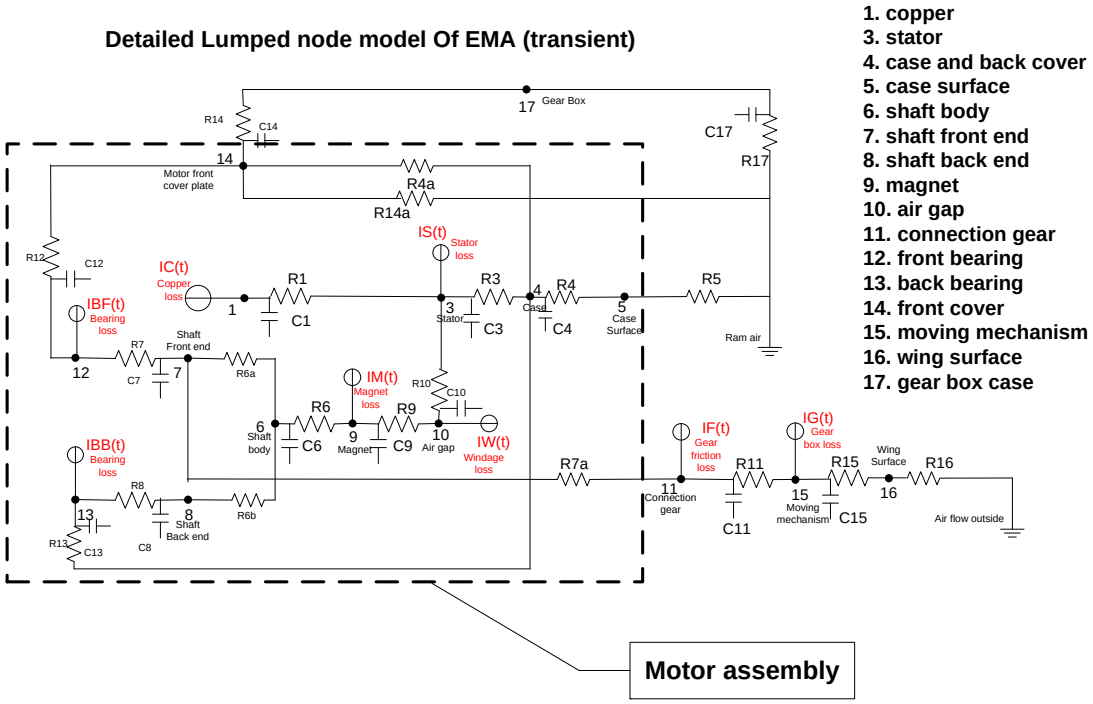

Fig. 3. Thermal lumped element model

This model is generic with multiple heat sources. However, for our simulations we considered only the copper loss which is the predominant heat source in our motor, and the other heat sources were set to zero. A few of the locations of the temperature nodes are shown in Fig. 4. Node 5 is the case surface and connects directly to the ambient air which serves as the heat sink.

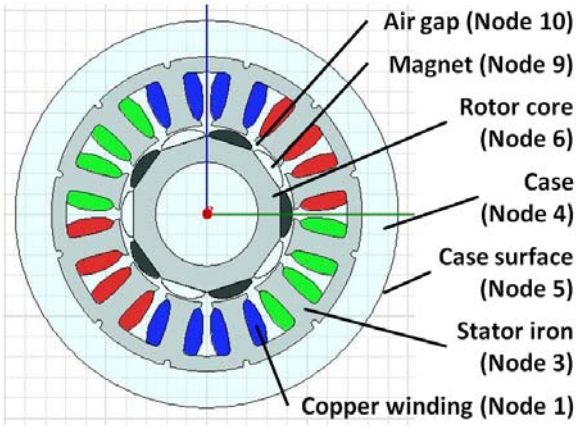

Fig. 4. Thermal node locations on motor

RESULTS

The input (desired) stroke profile and the motor's actual stroke profile are shown in Fig. 5. These profiles are made of 18 repetitions of a 5 minute profile.

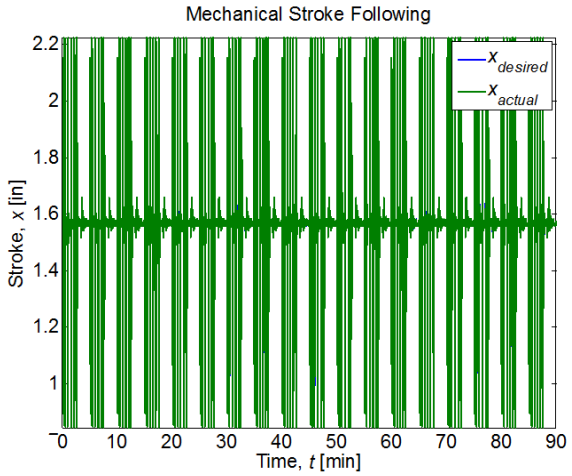

Fig. 5. Desired (blue) and actual (green) stroke profiles

The motor followed the desired stroke profile very well which is why barely any blue can be seen. The input load torque profile is shown in Fig. 6.

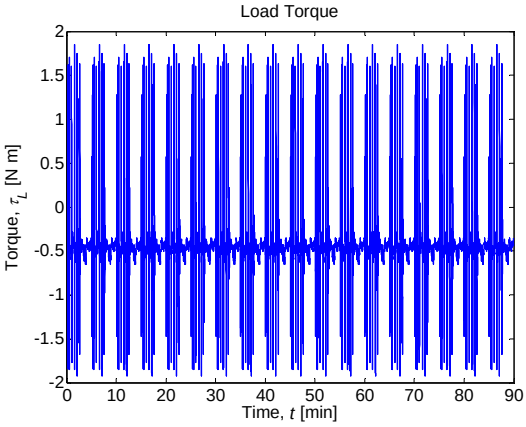

Fig. 6. Input load torque profile

We have found that the control design influences the amount of heat generated, especially the peak power lost to heat. When k_p was set to 0.05 s^{-1}, the mean power loss in the windings for the given input profile was about 0.99 W, the peak power loss was 12.05 W, and the error (a normalized sum of differences) in stroke (motor position) following was 0.0817%. In Fig. 7, we zoomed in on the stroke following to show 6 seconds. Here, a little overshoot can be seen. We will call this performance loose.

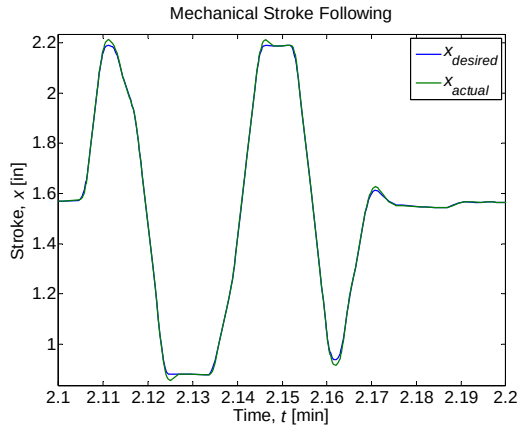

Fig. 7. Zoomed-in, 6-second view of loose stroke following (k_p = 0.05), desired (blue) and actual (green)

When the k_p value was increased to 0.7 s^{-1}, the mean power loss increased to about 1 W, the peak power loss rose to 20.65 W, but the stroke-following error dropped to 0.0248% (Fig. 8), meaning tighter control.

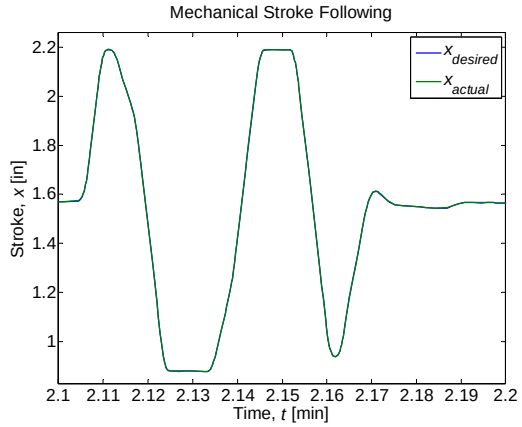

Fig. 8. Zoomed-in, 6-second view of tight stroke following (k_p = 0.7), desired (blue) and actual (green)

Although the mean power loss for these two simulations was about the same, there was a large difference in the peak power loss. In our simulations, we found that a k_p value set too high can cause additional power loss. The additional power loss comes from the motor working too hard to follow the input profile exactly.

The copper power loss (for k_p = 0.1 s^{-1}) in the motor for a 90 minute run is shown in Fig. 9.

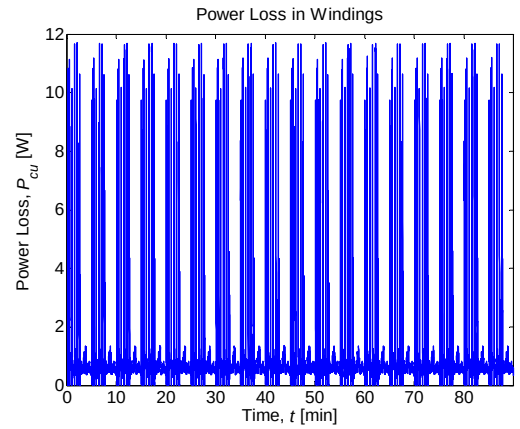

Fig. 9. Power loss in windings

The mean power loss was 0.98 W and the peak power loss was 11.71 W. It is worth noting that the peak power loss was 12 times higher than the mean power loss. This points to the necessity of an accurate, transient analysis versus a steady-state analysis since such surges of power can be the cause of motor failure.

Of great interest to power systems engineers are the electrical input power and the regen power. Our simulation outputs both of these quantities (Fig. 10).

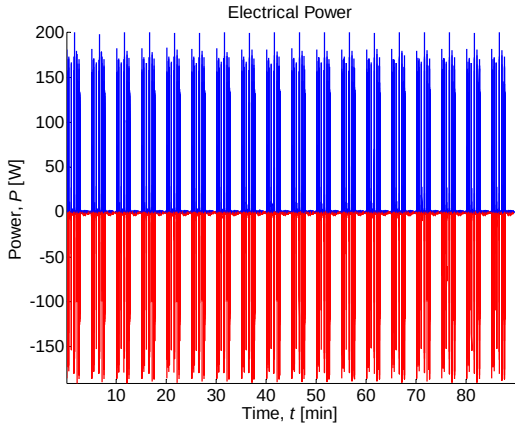

Fig. 10. Input electrical power (blue, positive) and regen power (red, negative)

The temperature profiles for various nodes are shown in Fig. 11. The highest temperatures pertain to the nodes closest to the copper windings. The ambient temperature was held at 22 °C.

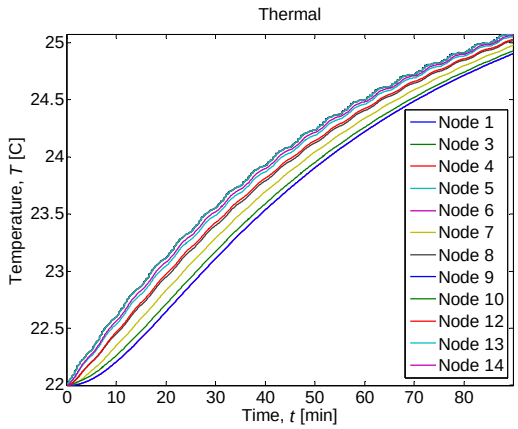

Fig. 11. Temperature profiles

Though this motor was put under a fairly light load, the critical aspect of nonlinear, transient simulation is being demonstrated. The 3 °C temperature rise can be simply explained by energy balance:

$$Q = \Delta T m c_p \qquad (27)$$

where the total energy lost to heat, Q, was

$$Q = 0.98\,\mathrm{W}\left(60\,\mathrm{s}\cdot 90\right) = 5292\,\mathrm{J} \qquad (28)$$

The total temperature rise, ΔT, was 3 °C; the mass of the motor, m, was 4.4 kg; and the specific heat capacity, c_p, was estimated as 400 J/kg °C. Therefore,

$$\Delta T m c_p = \left(3\,^{\circ}\mathrm{C}\right)\left(4.4\,\mathrm{kg}\right)\left(400\,\frac{\mathrm{J}}{\mathrm{kg}\,^{\circ}\mathrm{C}}\right) = 5280\,\mathrm{J} \qquad (29)$$

which is only a 0.23% difference from (28).

Although the speed of the computer will certainly affect the run-time ratio (real time/simulation time) as will the particular profile being simulated since highly transient portions of the input profiles require more computations, on the Gateway Centrino Duo 2.16 GHz laptop we used and with our inputs, the real-time ratio was over 20.

CONCLUSIONS

FEM is a powerful tool for characterizing motor parameters, and the combination of FEM and NL-LEMs provides for accurate, fast simulations of EMAs under transient conditions. This paper shows our integration of dynamic, nonlinear, lumped-element modeling, tuned by FEM, with field oriented control, copper loss and regenerative power calculation, and multi-node thermal modeling of the transfer of generated heat. Since our model runs so fast, it could be used in hardware-in-the-loop simulation. We detailed the primary dynamical equations of the motor,

and showed how these are used to simulate the motor and to build the control for the motor. We showed how the thermal, lumped-element network was laid out and where several of the network nodes were placed in the motor. And we showed how control can have an effect on the peak power loss which dissipates as heat and on the stroke-following performance. Finally, we showed how the inputs of desired stroke profile and load torque profile led to the outputs of actual motor stroke profile, input power and regenerative power profiles, and temperature profiles.

REFERENCES

1. Pointon, J. M., "Thermal Management of Electromechanical Actuation on an All-Electric Aircraft," MS thesis, Cranfield University, Bedfordshire, UK, 2007.
2. Shi, K. L., Chan, T. F., Wong, Y. K., Ho, S. L. "Modeling and Simulation of the Three-phase Induction Motor Using Simulink," *Int. J. Elect. Enging. Educ.*, Vol. 36, pp. 163-172., Manchester U.P., Great Britain, 1999.
3. Lipo, Thomas A., Consoli, Alfio, "Modeling and Simulation of Induction Motors with Saturable Leakage Reactances," *IEEE Transactions on Industry Applications*, Vol. IA-20, No. 1, pp. 180-189, 1981.
4. Soe, Nyein N., Yee, Thet T. H., Aung, S. S., "Dynamic Modeling and Simulation of Three-phase Small Power Induction Motor," *World Academy of Science, Engineering and Technology*, Vol. 42, No. 79, pp. 421-424, 2008.
5. Otto, Jens, "Dynamic Simulation of Electromechanical Systems using ANSYS and CASPOC," *2002 International ANSYS Conference*, ANSYS, 2002.
6. Roshen, Waseem, "Iron Loss Model for PM Synchronous Motors in Transportation," *2005 IEEE Conference on Vehicle Power and Propulsion*, pp. 4, ISBN: 0-7803-9280-9, 2005.
7. Dolinar, D., Weerdt, R. De, Freeman, E. M., "Calculation of Two-axis Induction Motor Model Parameters Using Finite Elements," *IEEE Transactions on Energy Conversion*, Vol. 12, No. 2, pp. 133-142, 1996.
8. Topcu, E. E., Kamis, Z.,Yuksel, I., "Simplified numerical solution of electromechanical systems by look-up tables," *Mechatronics*, Vol. 18, No. 10, pp. 559-565, Elsevier, 2008.
9. Fitzgerald, A. H., Kingsley, C. J., Umans, S. D., *Electric Machinery*, 6th ed., NY: McGraw-Hill, 2003.
10. Mohamed, M. A., Nagrial, M. H., "Modelling and Simulation of Vector-controlled Reluctance Motors Drive System," *International Conference on Simulation*, No. 457, pp. 380-384, ISBN: 0-85296-709-8, 1998.
11. Sun, Fengchun, Li, Jian, Sun, Liqing, Zhai, Li, Cguo, Fen, "Modeling and Simulation of Vector Control AC Motor Used by Electric Vehicle," *Journal of Asian Electric Vehicles*, Vol. 3, No. 1, pp. 669-672, Asian Electric Vehicle Society, 2005.
12. Demerdash, N. A., Gillott, D. H., "A New Approach for Determination of Eddy Current and Flux Penetration in Nonlinear Ferromagnetic Materials," *IEEE Trans. MAG-10*, pp. 682-685, 1974.
13. Ong, Chee-Mun, *Dynamic Simulation of Electric Machinery*, Prentice Hall, 1998.
14. Merzouki, R., Cadiou, J. C., "Estimation of backlash phenomenon in the electromechanical actuator," *Control Engineering Practice*, Vol. 13, No. 8, pp. 973-983, Elsevier, 2004.

15. Sefkat, Gursel, "Investigating Static and Dynamic Characteristics of Electromechanical Actuators (EMA) With MATLAB GUIs," *Computer Applications in Engineering Education*, Vol. 18, No. 2, pp. 383-396, Wiley, 2008.

CONTACT INFORMATION

David Woodburn, david.woodburn@knights.ucf.edu, University of Central Florida, Orlando, FL

ACKNOWLEDGMENTS

This research was made possible by AFRL funding under contract FA8650-09-2-2940.

NOTATION

VARIABLES

u	voltage [V]
i	current [A]
R	electrical resistance [Ω]
L	inductance [H]
λ	flux linkage [Wb]
θ	angle [rad]
ω	angular frequency [rad/s]
α	angular acceleration [rad/s^2]
τ	torque [N m]
p	number of poles
I	rotor's moment of inertia [N m s^2/rad]
c	rotor's coefficient of friction from windage and bearings [N m s/rad]
P	power [W]
e	error, [rad/s] or [rad/s^2] depending on the units of the subscript
k	scaling coefficient for error, [1/s] for k_p and [A s/rad] for k_i
h	heat transfer coefficient [W/K m^2]

dt infinitesimal time step [s]

Δt finite time step [s]

SUBSCRIPTS

d direct axis

q quadrature axis

s stator

me mechanical scale multiplied by number of pole pairs

PM permanent magnet

M motor

L load

a phase a

b phase b

c phase c

cu copper